IEEE Photonics Journal
An IEEE Photonics Society Publication

Open Access

Tunable Anisotropic Perfect Enhancement Absorption in Black Phosphorus-Based Metasurfaces

Volume 12, Number 3, June 2020

Bin Tang
Niegang Yang
Li Huang
Jiangbin Su
Chun Jiang

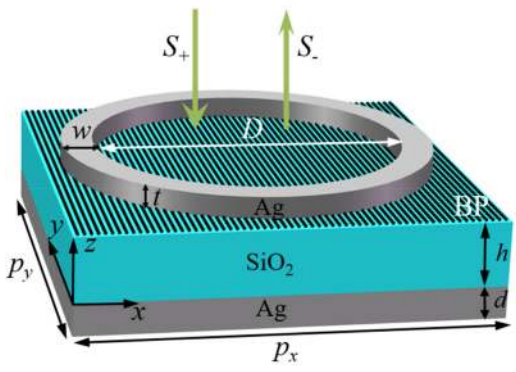

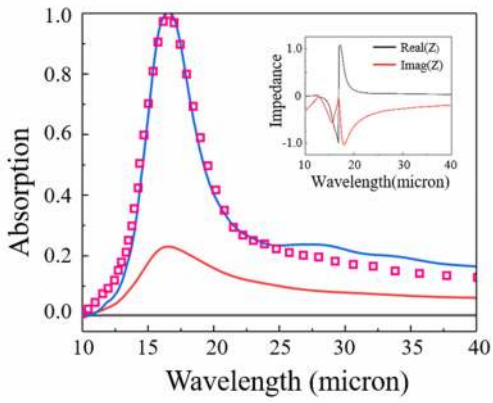

DOI: 10.1109/JPHOT.2020.2987157

IEEE photonics SOCIETY

IEEE

Tunable Anisotropic Perfect Enhancement Absorption in Black Phosphorus-Based Metasurfaces

Bin Tang,[1] **Niegang Yang**,[1] **Li Huang**,[1] **Jiangbin Su**,[1] **and Chun Jiang** [2]

[1]School of Mathematics & Physics, Changzhou University, Changzhou 213164, China
[2]State Key Laboratory of Advanced Optical Communication Systems and Networks, Shanghai Jiao Tong University, Shanghai 200240, China

DOI:10.1109/JPHOT.2020.2987157

Manuscript received March 16, 2020; revised April 6, 2020; accepted April 8, 2020. Date of publication April 15, 2020; date of current version April 29, 2020. The work was supported in part by the State Key Laboratory of Advanced Optical Communication Systems and Networks (2018GZKF03008).
Corresponding author: Bin Tang (E-mail: btang@cczu.edu.cn).

Abstract: In this work, we theoretically propose an anisotropic metasurface absorber, unit cell of which consists of a continuous monolayer black phosphorus (BP) sheet, sandwiched between a circular silver ring and a dielectric layer stacking on a silver substrate. Numerical results reveal that perfect enhancement absorption can be achieved in both armchair and zigzag directions, in which the resonant absorption peaks occur at different wavelengths due to the anisotropic property of BP. The calculated results by finite-difference time domain (FDTD) simulations have a good agreement with the coupled-mode theory. The physical mechanism of the perfect absorption is attributable to the critical coupling effect. Furthermore, the anisotropic perfect absorber not only exhibits tunable characteristics by varying the electron doping concentration, but also shows a wide-angle tolerance. In addition, our proposed absorber can achieve an arbitrary number of absorption bands by setting a suitable thickness of the dielectric layer. These results may have great potential applications in spectral imaging and photodetectors in the mid-infrared region.

Index Terms: Metasurface, perfect absorber, black phosphorus.

1. Introduction

In recent years, black phosphorus (BP) [1], [2], as a newly emerging two-dimensional (2D) anisotropic material with atomic-scale thickness, has received increasing attention due to the intriguing chemical, physical and electronic properties. In contrast to the other isotropic 2D materials, such as graphene [3], transition metal dichalcogenides (TMDs) [4], hexagonal boron nitride (h-BN) [5], BP has a wrinkled structure with a hexagonal lattice in the phosphorus atom, which can support the excitation of surface plasmons because of its unique in-plane anisotropic photonic and electrical properties [6]. Meanwhile, BP exhibits high carrier mobility (up to 50,000 $cm^2V^{-1}s^{-1}$ at 30 K) and remarkably tunable direct bandgap range from 0.3 eV in bulk to 2 eV in monolayer [7]. Therefore, as an alternative 2D material, BP can be regarded as a prospective semiconductor for applications in next generation electronics and photonics, and a suitable candidate for photonic applications, such as field effect transistors [8], [9], photovoltaic devices [10], [11], photodetectors [12], [13], spectral imaging [14], and ultrasensitive bio-sensing [15], and so on.

However, for the monolayer 2D materials, the low light absorption efficiency and weak sensitivity usually limit the practical applications. Thus, it is significant to enhance the light absorptivity or even obtain perfect absorption. As we know, BP with appropriate doping can support localized surface plasmons (LSPs) which are electromagnetic waves coupled to the carriers of BP. Excitation of LSPs can dramatically strengthen the interaction between the light and BP. In Ref. [16], T. Low, *et al.* demonstrated the realization of plasmonic excitations in BP, and the plasmon frequency can be tuned by adjusting the carrier concentration and the coupling strength. Liu *et al.* [17] theoretically elaborated the properties of LSPs in monolayer BP using periodic nanoribbon. Nong *et al.* [18] theoretically studied the hybridization of graphene surface plasmons and BP surface plasmons, and the maximum absorption rate is ∼20%. Ni *et al.* [19] explored the excitation of BP plasmons by depositing a square BP array on top of a dielectric substrate, resulting in enhanced absorption around 30%. Recently, a nearly perfect infrared absorber was proposed by inserting a monolayer BP into the resonator composing of a metal film and a dielectric Bragg reflector [20]. In addition, other proposals for improvement of the absorption efficiency were demonstrated by designing system with multilayered BP nanoribbon or multilayered BP/dielectric sandwich-like structure [21]–[23], which directly complicates the fabrication process. Also, the coherent quasi-perfect absorption theory was proposed by using a non-resonant monolayer BP [24], [25], which needs additional configurations to obtain a proper phase modulation. More recently, a total absorption scheme was introduced to achieve the perfect absorption in 2D materials based on coupled-mode theory [26]. For example, Qing *et al.* proposed a perfect absorber by critical coupling of a monolayer BP with guided resonance of a photonic crystal waveguide slab to enhance light absorption at terahertz frequencies [27], and investigated the strong coupling of multiple resonance modes in a BP-hybrid system [28]. However, although the absorbance is considerably high for a single 2D materials among the above works, it is still insufficient for high-performance optoelectronic devices in a wide broad spectral regime.

In this paper, we theoretically propose an anisotropic metasurface absorber consisting of a continuous monolayer BP sheet sandwiched between a circular silver ring array and a dielectric layer stacking on a silver mirror, which can achieve nearly perfect absorption in both armchair and zigzag directions. The calculated results by finite-difference time domain (FDTD) simulations match well with the coupled-mode theory. Meanwhile, the compound architecture exhibits strong anisotropic spectral responses and perfect absorption enhancement that are not available in either individual BP film or silver rings, thus providing an avenue in designing anisotropic meta-devices in mid-infrared regimes. The mechanism of the perfect absorption is attributable to the critical coupling effect. Moreover, the proposed perfect absorber not only exhibits tunable characteristics by altering the electron doping of BP layer, but also shows wide-angle tolerance under a large incident angle. In addition, our proposed absorber can achieve an arbitrary number of absorption bands by setting a suitable thickness of the dielectric layer, which may have some potential applications in spectral imaging and photodetectors.

2. Theoretical Model and Structural Design

For a monolayer BP, the complex surface conductivity can be described by using a semi-classical Drude model [17]:

$$\sigma_{jj} = \frac{\mathrm{i}D_j}{\pi\left(\omega + \frac{\mathrm{i}\eta}{\hbar}\right)}, \quad D_j = \frac{e^2\pi n}{m_j}, \tag{1}$$

where $\mathrm{i} = \sqrt{-1}$, D_j is the Drude weight, $j = x, y$ represents the position along the armchair (x) and zigzag (y) direction, respectively. ω is the incident light frequency, and $\bar{\mathrm{h}}$ is the reduced Planck's constant. η describes the relaxation rate, and n is the parameter describing the electron concentration, and the electron mass m_j along armchair direction and zigzag direction can be

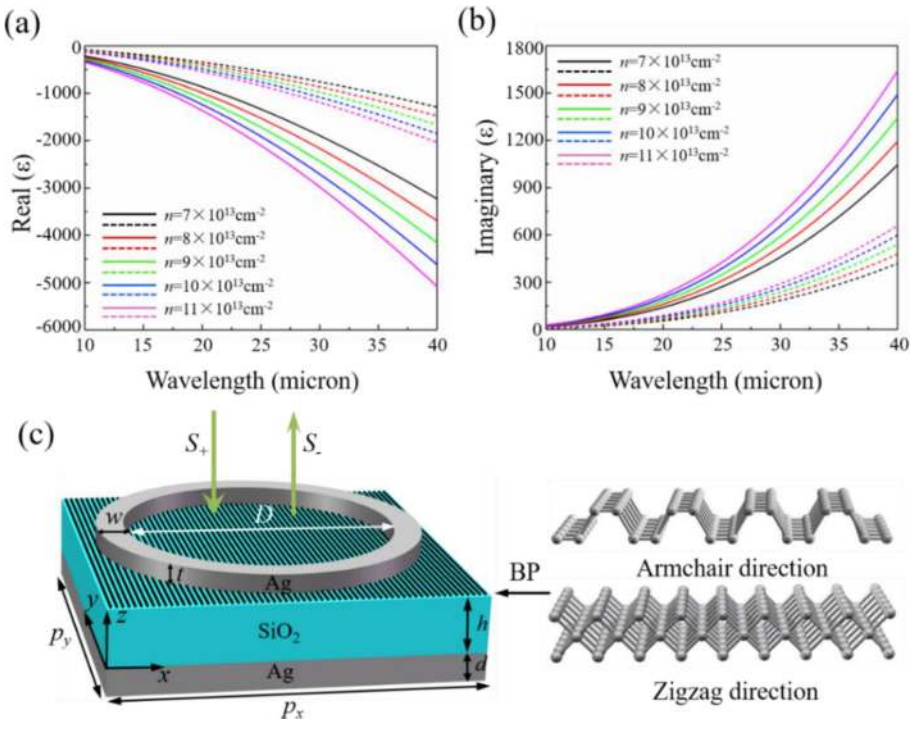

Fig. 1. (a) The real part and (b) imaginary parts of the effective permittivity for different electron doping concentration. The solid lines represent the effective permittivity of BP along the armchair direction, and the dashed lines are results along the zigzag direction. (c) The schematic diagram of the compound absorber, unit of which consists of a continuous monolayer BP sheet, sandwiched between a circular silver ring and a dielectric layer stacking on a silver substrate. In this design, the geometrical parameters are listed as follows: $D = 660$ nm, $w = 35$ nm, $t = 30$ nm, $h = 1500$ nm, $d = 300$ nm, and the periodicity of this structure $p_x = \mathrm{p_y} = 700$ nm.

defined by [17], [29]:

$$m_x = \frac{\hbar}{\frac{2\gamma^2}{\Delta} + \eta_c}, \quad m_y = \frac{\hbar^2}{2\nu_c}. \tag{2}$$

In equation (2), the related parameters are set as follows: band gap$\Delta = 2$eV, $\eta_c = \hbar^2/0.4m_0$, $\nu_c = \hbar^2/1.4m_0$, where electron mass $\mathrm{m_0} = 9.10938 \times 10^{-31}$ kg. $\gamma = 4a/\pi$, and π/a denotes the width of Brillouin zone, and $a = 0.223$ nm is the scale length of monolayer BP. It should be noted that the band parameters are highly sensitive to the number of BP layers due to the remarkably tunable direct band gap of BP, and a small change can obviously alter the anisotropic effective mass. The anisotropic dielectric function of BP reads:

$$\varepsilon_{jj} = \varepsilon_r + \frac{\mathrm{i}\sigma_{jj}}{\varepsilon_0 \omega \tau}, \tag{3}$$

where the relative permittivity $\varepsilon_r = 5.76$, the permittivity of free space $\varepsilon_0 = 8.854 \times 10^{-12}$ F·m^{-1} and the thickness of a monolayer BP film τ takes the value of 1 nm. Given the relaxation rate $\eta =$ 10 meV, we calculate the real and imaginary parts of the effective surface conductivity for different electron doping as shown in Fig. 1(a) and Fig. 1(b), respectively. From these figures, one can see that the real part of the effective permittivity of BP along the armchair direction is smaller than the zigzag direction for the same electron doping. By contrast, the imaginary part of the effective permittivity in the armchair direction is larger than the one in the zigzag direction. As a result, the optical loss in the armchair direction is larger than the zigzag direction. And the effective mass in

the armchair direction is smaller than the zigzag direction. Therefore, comparing with the zigzag direction, BP has larger absorption and higher resonance frequency in the armchair direction.

The schematic diagram for the unit cell of the designed architecture is illustrated in Fig. 1(c), which is composed of a continuous monolayer BP sheet, sandwiched between a circular silver ring and a dielectric layer stacking on a silver substrate. The bottom silver layer behaves as a thick metal mirror, which can block the transmission of the incident light. The related geometrical parameters are given in the caption of Fig. 1. The dielectric layer is assumed to be SiO_2 with the refractive index of 1.45. The permittivity of silver is taken as Drude mode: $\varepsilon_m(\omega) = \varepsilon_\infty - {\omega_p}^2/(\omega^2 + i\omega\gamma)$, where ω is the angular frequency, and the plasma frequency is $\varepsilon_p = 1.39 \times 10^{16}$ rad/s, the scattering rate is $\gamma = 2.7 \times 10^{13}$ rad/s, and the high-frequency constant is $\varepsilon_\infty = 3.4$, separately. The full-field electromagnetic wave calculations were performed by three-dimensional Finite-Difference Time Domain (FDTD) method. In simulations, the normally incident plane wave is along the negative direction of the *z*-axis. In addition, the periodic boundary conditions were applied in both *x* and *y* direction, and the perfectly matched absorbing boundary conditions were utilized to absorb all the light coming out the boundaries along the propagation direction. The spectral absorptivity is calculated by $A = 1 - R - T$, where R and T represents the reflection and transmission, respectively. In our calculations, the transmission T is zero in that the thickness of the metal is much greater than the skin depth of incident light in the metal. Therefore, the absorptivity can be simplified by $A = 1 - R$. It is also noted that the system works as such configuration of a single port coupled with a resonator without the transmission channel. According to the coupled-mode theory (CMT) [30], [31], the system can be described by the following equations:

$$\frac{da}{dt} = (i\omega_0 - \delta - \gamma) + \sqrt{2\gamma}S_+, \tag{4}$$

$$S_- = -S_+ + \sqrt{2\gamma}a, \tag{5}$$

where a is the resonant amplitude, S_+ and S_- represent the amplitudes of input and outgoing wave, respectively. δ, γ, ω_0 are intrinsic loss, external leakage rate and resonant frequency, separately. The reflection coefficient of the model is:

$$r = \frac{S_-}{S_+} = \frac{i(\omega - \omega_0) + \delta - \gamma}{i(\omega - \omega_0) + \delta + \gamma}, \tag{6}$$

and the absorption coefficient is:

$$A = 1 - |r|^2 = \frac{4\delta\lambda}{(\omega - \omega_0)^2 + (\delta + \gamma)^2}. \tag{7}$$

In addition, the impedance of the structure system should match with that of the free space ($Z = Z_0 = 1$) under critical coupling conditions. The effective impedance of the system can be expressed as [32]:

$$Z = \sqrt{\frac{(1 + S_{11})^2 - S_{21}^2}{(1 - S_{11})^2 - S_{21}^2}}. \tag{8}$$

where S_{11} and S_{21} represent the scattering parameters relevant to reflection and transmission coefficients, respectively.

3. Results and Discussions

Fig. 2 shows the optical absorption spectra for the compound metasurface structure at normal incidence with polarization along armchair direction and zigzag direction, respectively. From Fig. 2(a), one can see that the absorption efficiency tends to zero for the structure without BP sheet as shown by the black line. By contrast, the absorption spectrum for the structure without silver ring has a resonant absorption peak with efficiency of ~20% at the wavelength of 16.53 μm indicated by the red curve. In particular, the optical absorption spectrum shown by blue curve exhibits a

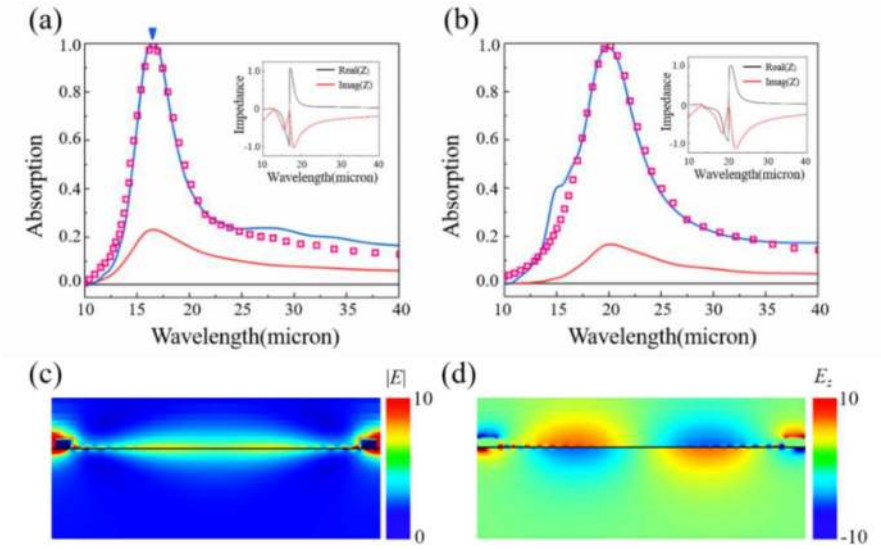

Fig. 2. (a) Simulated optical absorption spectra (blue curve) for the proposed compound structure along the armchair direction, without circular silver ring (red curve) and without BP sheet (black curve), separately; (b) Simulated optical absorption spectra (blue curve) for the proposed compound structure along the zigzag direction, without circular silver ring (red curve) and without BP sheet (black curve), separately. Pink curves in both (a) and (b) are the absorption spectra from the CMT theory. The insets in Fig. 2(a) and Fig. 2(b) represent the real and imaginary parts of the effective impedance along the armchair direction and zigzag direction, respectively. (c) The electric field |E| and (d) E_z distribution at the resonant peak indicated by the blue del in Fig. 2(a). The electron doping concentration is set to $n = 9 \times 10^{13}$ cm^{-2}.

nearly perfect absorption with 99.8% at the resonant wavelength when combining the circular silver ring and the monolayer BP sheet along armchair direction (*x*-direction). Meanwhile, when the polarization direction of light is along the zigzag direction (*y*-direction) of BP, the whole compound structure also manifests an obvious enhancement absorption with ∼98.36% at the wavelength of 20.12 μm indicated by the blue line as shown in Fig. 2(b). Compared with the armchair direction, the resonant absorption wavelength in Fig. 2(b) exhibits a red-shift because the larger mass along the zigzag direction has a lower resonance frequency. In addition, the absorption spectra from CMT theory are given as a comparison with the FDTD results shown by the pink curve in Fig. 2(a) and Fig. 2(b). It is clearly shown that the results have a great agreement between CMT theory and FDTD simulated results, which demonstrate the validity of the CMT for the single port system. Here the related fitted parameters list as follows: $\delta = 1.37$ THz, $\gamma = 1.55$ THz in Fig. 2(a) and $\delta = 1.49$ THz, $\gamma = 1.25$ THz in Fig. 2(b). According to the CMT, the total quality factor can be defined as $Q = f_0/\Delta f$, which reaches about 3.16 at the resonant peak in Fig. 2(a). The factor of the intrinsic loss $\delta$and external leakage γ of the resonant mode can be defined as $Q_\delta = \omega_0/2\delta$ and $Q_\gamma = \omega_0/2\gamma$, respectively. Thus, the quality factor can be obtained by $Q_{\mathrm{CMT}} = Q_\delta \,.\, Q_\gamma/(Q_\delta + Q_\gamma)$ in theory, which is 3.01. From the above calculations, the value of the theoretical calculation Q and the numerical result Q_{CMT} are almost identical, indicating that the perfect absorption of the configuration can be ascribed to the critical coupling. In addition, according to Eq. (8), the effective impedance of the proposed absorber is calculated as shown in the inset of Fig. 2(a). The effective impedance at the resonant frequency is $Z = 1.028 - 0.033$i when the polarization is along the armchair direction. The derived effective impedance shows a good match with the impedance of free space, which means the reflection can be effectively suppressed, thus resulting in the critical coupling and perfect absorption.

To explore the underlying physics behind the perfect enhancement absorption, Fig. 2(c) and Fig. 2(d) give the distributions of electric field E and amplitude of z-component E_z at the peak wavelength indicated by the blue del in Fig. 2(a). It is observed that localized surface plasmons

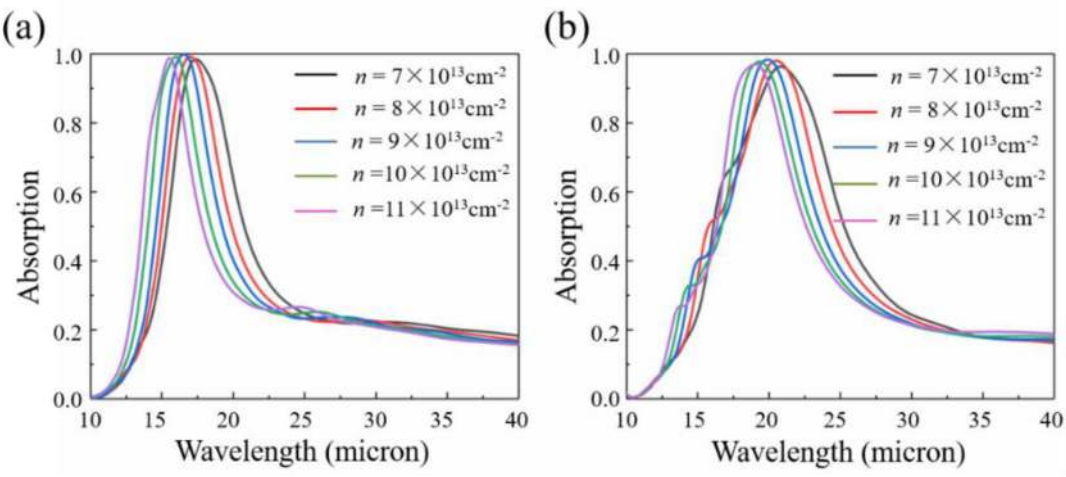

Fig. 3. Absorption curves at different electron doping for the polarization along (a) armchair direction and (b) zigzag direction.

resonance modes are excited in the edge of the metal ring and the electric field concentrates at the BP interface. And the positive and negative dipole responses can be easily discovered from the vertical distribution of E_z component, indicating the excitation of localized BP surface plasmon modes. Under the resonant excitations, there exhibits a strong interaction between localized surface plasmons in metal rings and BP surface plasmon modes. For the single port system, the total absorbance occurs only at the condition of critical coupling when the internal loss rate equals to the radiation rate without reflection at the resonant wavelength. The physical mechanism derives from the destructive interference between light coupling with localized surface plasmons and light directly reflected from the surface of the system. Meanwhile, the formed Fabry-Pérot cavity between BP sheet and metal substrate further strengthens the interaction of multiple reflected light inside the spacer. Thus, the entire system generates a strong absorption of photon energy, allowing the structure to be a perfect absorber. Actually, the spacer thickness also plays a major role in determining the resonant absorption wavelength of the Fabry-Pérot cavity, which will be discussed in the last part of this paper.

Furthermore, to investigate the tunable properties of the BP absorbers. Fig. 3 presents the impacts of electron doping on the optical absorption spectra for polarization along armchair direction and zigzag direction. As shown in Fig. 3, when the electron doping is increased from 7×10^{13} cm^{-2} to 11×10^{13} cm^{-2}, the optical absorption spectrum has a slight blue-shift for both polarization directions, which can be elucidated by the facts that the real part of the effective permittivity of BP becomes smaller with larger electron doping. The smaller effective mass of BP indicates higher resonance frequency. Thus, the proposed absorber can work at different wavelengths and guarantee actively tuning with high absorption efficiency in a wide range of wavelength. Meanwhile, since the imaginary part of the effective permittivity in the armchair direction is larger than the one in the zigzag direction, it suggests that the optical loss in armchair direction is higher and the resonance line width is slightly narrower. Thus, the absorber has a higher absorption efficiency and higher resonance frequency in the armchair direction comparing with the absorption in the zigzag direction, manifesting the anisotropic absorption of the absorber. Therefore, the anisotropic perfect absorber can be tuned by changing the BP electron doping.

In addition, Fig. 4 depicts the absorption spectra as a function of polarization angle and wavelength at normal incidence. Here the polarization angle refers to the electric field polarization direction of incident light with respect to the x-axis. From Fig. 4, it is observed that the optical absorption spectra exhibit a polarization-dependent property even though the system is circularly symmetric. As the polarization angle is increased gradually from 0° to 45°, the absorbance

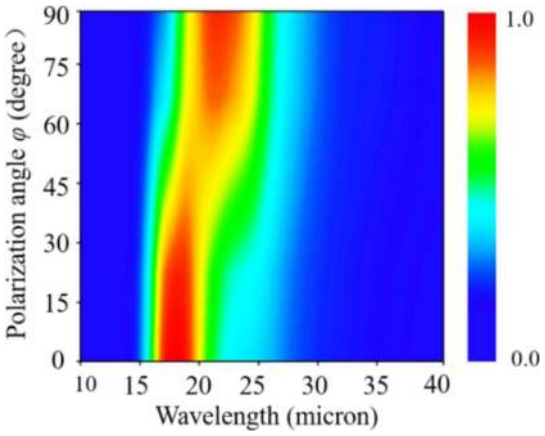

Fig. 4. Calculated optical absorption spectra as functions of polarization angle and the wavelength the when the light is normal illumination.

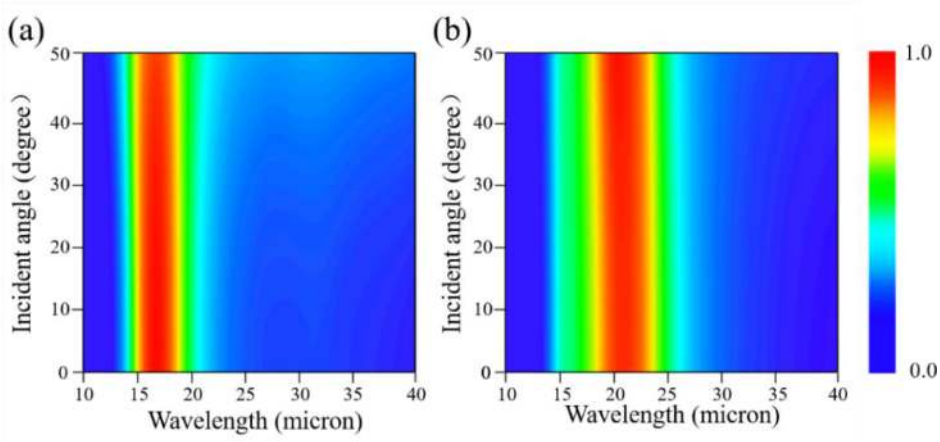

Fig. 5. Absorption spectra versus different incidence angle for the polarization along (a) armchair direction and (b) zigzag direction.

decreases by degree at the corresponding resonant wavelength. On the contrary, the absorbance exhibits an inverse process with further increasing of the polarization angle. Meanwhile, the positon of the resonant wavelength has a slight red-shift. Particularly, when the polarization angle $\varphi = 0°$, the optical absorption spectrum has a perfect absorption, which corresponds to the polarization of plane waves along *x*-direction (armchair direction). By contrast, when the polarization angle $\varphi = 90°$, that is the polarization of plane waves along *y*-direction (zigzag direction), the absorption spectrum selectively appears to be of a lower absorptivity (nearly perfect absorption) due to the anisotropy of BP. Obviously, these results further demonstrate the characteristic of anisotropic absorbance of the proposed absorber.

Next, the absorption performance of the absorber under oblique incidence is also investigated. Fig. 5 calculates the optical absorption spectra as functions of wavelength and incident angle. From Fig. 5, when the incident angle is increased from 0° to 50°, the resonant peaks can remain at a nearly perfect and stable absorption efficiency while having a large incident angle. The absorption performance in both armchair and zigzag direction is insensitive to the incident angle. Meanwhile, the positions of resonant absorption peaks almost keep invariant for both polarization directions. The difference of resonant absorption efficiency and peak positions in both polarization directions comes from the anisotropic characteristic of BP-based absorber. Therefore, the proposed absorber

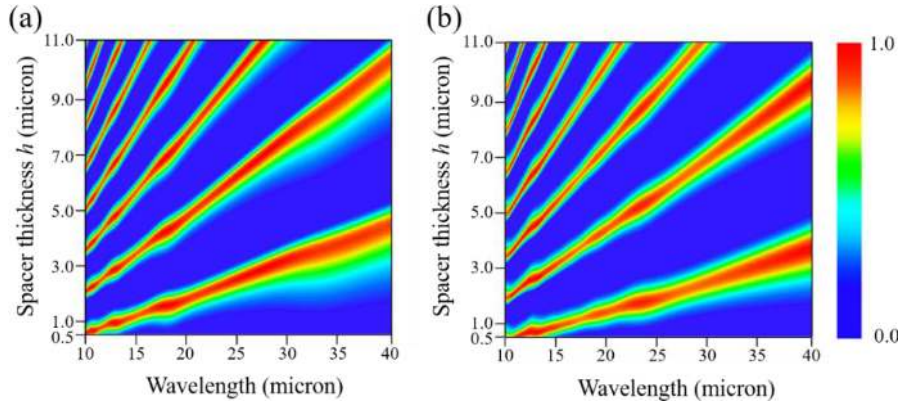

Fig. 6. Absorption spectra versus different thicknesses of dielectric layer along (a) armchair direction and (b) zigzag direction.

shows a remarkable tolerance for the absorption performance under a wide incident angle for polarizations of light along armchair direction and zigzag direction.

Finally, we revisit the effect of structure parameter (e.g., the spacer thickness h) on the resonant absorption of the proposed absorber. From Fig. 6, one can find that the resonant absorption of the absorber can be developed from one to multiple peaks with nearly perfect absorbance simultaneously in armchair and zigzag direction. The multiband absorption phenomenon resulting from the BP-metal reflector Fabry-Pérot cavity can be interpreted by interference theory [33]. In the interference model, the light is reflected back and forth between the BP sheet and metal substrate, with a complex propagation phase $\tilde{\beta} = \sqrt{\tilde{\varepsilon}} k_0 h$, where $\tilde{\varepsilon}$ is the permittivity of the spacer, k_0 is the free space wavenumber, and h is the spacer thickness. The absorbance can be retrieved through $A(\omega) = 1 - |\tilde{r}(\omega)|^2$, where $\tilde{r}(\omega)$is the total reflection resulting from superposition of multiple reflections. Obviously, the spacer thickness h plays a major role in determining the wavelength of Fabry-Pérot resonances. It is clearly seen from Fig. 6 that the spacer thickness directly affects the number of absorption peaks. As the spacer thickness h increases gradually, the number of peaks increases linearly and the frequency of each order resonance decreases correspondingly. For example, as h increases from 1 to 9 μm, the number of absorption peaks reaches from 1 to 5 at the wavelength range of 10 $\sim$ 40 μm, correspondingly. The maximum absorbance occurs at the constructive interference with phase condition of $2\tilde{\beta} + \phi + \pi \approx 2m\pi$, where ϕ represents the reflection phase shift on the BP-dielectric interface. Therefore, we can conclude that the proposed absorber can achieve an arbitrary number of absorption bands in the mid-infrared region by setting a suitable thickness of the dielectric layer.

4. Conclusions

In summary, we theoretically propose and numerically demonstrate a tunable wide-angle anisotropic perfect absorber based on BP-based metasurfaces, which consists of a circular silver ring array, a dielectric layer sandwiched between BP sheet and a metal mirror. The compound architecture exhibits strong anisotropic spectral responses and perfect enhancement absorption for the polarization along armchair and zigzag direction of BP, which are not available in either individual BP film or silver rings. The calculated results by FDTD simulations have a good agreement with the coupled-mode theory. The total absorption of the configuration at the resonant wavelength can be ascribed to the critical coupling effect. Furthermore, the proposed perfect absorber not only exhibits tunable characteristics by varying the electron doping concentration, but also shows a wide-angle tolerance which is free from changing the incident angle. In addition, our proposed absorber can achieve an arbitrary number of absorption bands by setting a suitable thickness of the dielectric layer, which may have some potential applications in spectral imaging and photodetectors.

References

[1] F. Xia, H. Wang, and Y. Jia, "Rediscovering black phosphorus as an anisotropic layered material for optoelectronics and electronics," *Nature Commun.*, vol. 5, 2014, Art. no. 4458.
[2] X. Wang *et al.*, "Highly anisotropic and robust excitons in monolayer black phosphorus," *Nature Nanotech.*, vol. 10, no. 6, pp. 517–521, 2015.
[3] Y. Zhu *et al.*, "Graphene and graphene oxide: Synthesis, properties, and applications," *Adv. Mater.*, vol. 22, no. 35, pp. 3906–3924, 2010.
[4] A. Splendiani *et al.*, "Emerging photoluminescence in monolayer MoS2," *Nano Lett.*, vol. 10, no. 4, pp. 1271–1275, 2010.
[5] L. Song *et al.*, "Large scale growth and characterization of atomic hexagonal boron nitride layers," *Nano Lett.*, vol. 10, no. 8, pp. 3209–3215, 2010.
[6] X. Ling *et al.*, "Anisotropic electron-photon and electron-phonon interactions in black phosphorus," *Nano Lett.*, vol. 16, no. 4, pp. 2260–2267, 2016.
[7] F. Xiong, J. Zhang, Z. Zhu, X. Yuan, and S. Qin, "Strong anisotropic perfect absorption in monolayer black phosphorous and its application as tunable polarizer," *J. Opt.*, vol. 19, no. 7, 2017, Art. no. 075002.
[8] W. Dickerson *et al.*, "Phosphorus oxide gate dielectric for black phosphorus field effect transistors," *Appl. Phys. Lett.*, vol. 112, no. 17, 2018, Art. no. 173101.
[9] J. Xu, J. Jia, S. Lai, J. Ju, and S. Lee, "Tunneling field effect transistor integrated with black phosphorus-MoS2 junction and ion gel dielectric," *Appl. Phys. Lett.*, vol. 110, no. 3, 2017, Art. no. 033103.
[10] M. Buscema, D. J. Groenendijk, G. A. Steele, H. S. van der Zant, and A. Castellanos-Gomez, "Photovoltaic effect in few-layer black phosphorus PN junctions defined by local electrostatic gating," *Nature Commun.*, vol. 5, 2014, Art. no. 4651.
[11] A. Shang and X. Li, "Photovoltaic devices: Opto-electro-thermal physics and modeling," *Adv. Mater*, vol. 29, no. 8, pp. 1603492-1–1603492-8, 2017.
[12] P. K. Venuthurumilli, P. D. Ye, and X. Xu, "Plasmonic resonance enhanced polarization-sensitive photodetection by black phosphorus in near infrared," *ACS Nano*, vol. 12, no. 5, pp. 4861–4867, 2018.
[13] J. Miao *et al.*, "Single Pixel Black Phosphorus Photodetector for Near-Infrared Imaging," *Small*, vol. 14, no. 2, pp. 1702082-1–1702082-7, 2018.
[14] M. Engel, M. Steiner, and P. Avouris, "Black phosphorus photodetector for multispectral, high-resolution imaging," *Nano Lett.*, vol. 14, no. 11, pp. 6414–6417, 2014.
[15] Y. Yuan *et al.*, "Highly anisotropic black phosphorous-graphene hybrid architecture for ultrassensitive plasmonic biosensing: Theoretical insight," *2D Mater.*, vol. 5, no. 2, 2018, Art. no. 025015.
[16] T. Low *et al.*, "Plasmons and screening in monolayer and multilayer black phosphorus," *Phys. Rev. Lett.*, vol. 113, no. 10, 2014, Art. no. 106802.
[17] Z. Liu and K. Aydin, "Localized surface plasmons in nanostructured monolayer black phosphorus," *Nano Lett.*, vol. 16, no. 6, pp. 3457–3462, 2016.
[18] J. Nong *et al.*, "Strong coherent coupling between graphene surface plasmons and anisotropic black phosphorus localized surface plasmons," *Opt. Express*, vol. 26, no. 2, pp. 1633–1644, 2018.
[19] X. Ni, L. Wang, J. Zhu, X. Chen, and W. Lu, "Surface plasmons in a nanostructured black phosphorus flake," *Opt. Lett.*, vol. 42, no. 13, pp. 2659–2662, 2017.
[20] D. Dong *et al.*, "Designing a nearly perfect infrared absorber in monolayer black phosphorus," *Appl. Opt.*, vol. 58, no. 14, pp. 3862–3869, 2019.
[21] Y. Zhu, B. Tang, and C. Jiang, "Tunable ultra-broadband anisotropic absorbers based on multi-layer black phosphorus ribbons," *Appl. Phys. Express*, vol. 12, no. 3, 2019, Art. no. 032009.
[22] Y. Cai, K.-D. Xu, N. Feng, R. Guo, H. Lin, and J. Zhu, "Anisotropic infrared plasmonic broadband absorber based on graphene-black phosphorus multilayers," *Opt. Express*, vol. 27, no. 3, pp. 3101–3112, 2019.
[23] S. Xiao *et al.*, "Tunable anisotropic absorption in hyperbolic metamaterials based on black phosphorous/dielectric multilayer structures," *J. Lightw. Techn.*, vol. 37, no. 13, pp. 3290–3297, 2019.
[24] X. Wang *et al.*, "Tunable terahertz/infrared coherent perfect absorption in a monolayer black phosphorus," *Opt. Express*, vol. 26, no. 5, pp. 5488–5496, 2018.
[25] T. Guo and C. Argyropoulos, "Tunable and broadband coherent perfect absorption by ultrathin black phosphorus metasurfaces," *J. Opt. Soc. Amer. B*, vol. 36, no. 11, pp. 2962–2971, 2019.
[26] T. Liu, X. Jiang, C. Zhou, and S. Xiao, "Black phosphorus-based anisotropic absorption structure in the mid-infrared," *Opt. Express*, vol. 27, no. 20, pp. 27618–27627, 2019.
[27] Y. M. Qing, H. F. Ma, and T. J. Cui, "Tailoring anisotropic perfect absorption in monolayer black phosphorus by critical coupling at terahertz frequencies," *Opt. Express*, vol. 26, no. 25, pp. 32442–32450, 2018.
[28] Y. M. Qing, H. F. Ma, and T. J. Cui, "Strong coupling between magnetic plasmons and surface plasmons in a black phosphorus-spacer-metallic grating hybrid system," *Opt. Lett.*, vol. 43, no. 20, pp. 4985–4988, 2018.
[29] L. Tony *et al.*, "Plasmons and screening in monolayer and multilayer black phosphorus," *Phys. Rev. Lett.*, vol. 113, no. 10, 2014, Art. no. 106802.
[30] J. R. Piper and S. Fan, "Total absorption in a graphene monolayer in the optical regime by critical coupling with a photonic crystal guided resonance," *ACS Photon.*, vol. 1, no. 4, pp. 347–353, 2014.
[31] F. Shanhui, S. Wonjoo, and J. D. Joannopoulos, "Temporal coupled-mode theory for the Fano resonance in optical resonators," *J. Opt. Soc. Amer. A*, vol. 20, no. 3, pp. 569–572, 2003.
[32] D. R. Smith, D. C. Vier, T. Koschny, and C. M. Soukoulis, "Electromagnetic parameter retrieval from inhomogeneous metamaterials," *Phys. Rev. E*, vol. 71, no. 3, 2005, Art. no. 036617.
[33] H.-T. Chen, "Interference theory of metamaterial perfect absorbers," *Opt. Express*, vol. 20, no. 7, pp. 7165–7172, 2012.